Original article

One-step synthesis of magnetic N-doped carbon nanotubes derived from waste plastics for effective Cr(VI) removal

Song Cheng [a,c], Xiangwang Zeng [a], Peng Liu [b,*]

[a] *College of Chemistry and Chemical Engineering, Henan Polytechnic University, Jiaozuo 454003, China*
[b] *School of Vanadium and Titanium, Panzhihua University, Panzhihua 617000, China*
[c] *Collaborative Innovation Center of Coal Work Safety and Clean High Efficiency Utilization, Jiaozuo 454003, China*

A B S T R A C T

The magnetic nitrogen-doped carbon nanotube is prepared by one-pot using waste plastics as feedstock in the existence of the urea and $Fe(NO_3)_3$ for Cr(VI) removal form wastewater. The characterization analysis indicates that the nitrogen is successfully doped on the magnetic nitrogen-doped carbon nanotube with specific surface area of the 158.71 m^2/g and saturation magnetization of the 36.47 emu g^{-1}. The existence of the nitrogen group and Fe_3C contributes to Cr(VI) removal by complexation and reduction with adsorption capacity of the 27.47 mg g^{-1}. The adsorption data is fitting well with the Pseudo-second order model, demonstrating chemisorption of Cr (VI). The Cr(VI) removal mechanism analysis indicates that Fe^0, Fe^{2+}, H*, oxygen-containing group and nitrogen-containing group are crucial to Cr(VI) removal. The key mechanism of the enhanced Cr (VI) removal is the reductive capacity by dissolved Fe^{2+}, which accounts for 23.6 % of the overall Cr(VI) removal. The magnetic nitrogen-doped carbon nanotube is prepared from waste plastic for Cr (VI) removal from wastewater.

1. Introduction

Nowadays, heavy metals in water bodies have posed serious threat to the ecosystem (Afzali and Fayazi, 2016; Fayazi, 2020; Guo et al., 2024). Cr(VI) is one of the heavy metals in the water bodies with the highly toxic and non-biodegradable (Fayazi and Ghanbarian, 2020). The wastewater sludge accumulated and discharged from these industries are the major source of Cr(VI) in the environment (Zhao et al., 2024). The Cr(VI) is carcinogenic, toxic and teratogenic to human health (Xu et al., 2024). The Cr(VI) readily enters the body through a number of routes, including the inhalation and dermal contact. Any discharge of Cr (VI) into water bodies can cause the poisonous and harmful effects for humans and ecological environment. Generally, Cr(VI) crosses cell membranes through the transport system, and some of the substances produced in the process of reaction can bind with the DNA and cause cellular damage to cells (Myers, 2012). Therefore, controlling the concentration of Cr(VI) in water bodies is important to reduce the risk of biopathological damage. According to the World Health Organization (WHO) standards, the concentration of Cr(VI) in drinking water should not exceed 50 µg/L (Fida et al., 2015). Several treatment methods such as electrochemical, biological treatment, adsorption and photocatalysis are used for removal of Cr(VI) from wastewater (Fu and Wang, 2011;

Yang et al., 2021). However, adsorption is a simple and effective method among these costly and complex methods. Many adsorbents including activated carbon, carbon nanotubes and biochar have been prepared for Cr(VI) removal from wastewater (Fu and Wang, 2011; Zhao et al., 2021; Zou et al., 2021; Guan et al., 2024).

Due to its unique structure and properties, carbon nanotubes have been extensively used for Cr(VI) removal from wastewater. For example, Ma et al. (2024) prepared the zirconium oxide–carbon nanotubes for Cr (VI) removal from wastewater with adsorption capacity of 97.39 mg g^{-1} (Ma et al., 2024). Kim et al. (2024) used the TiO_2/Multi-walled carbon nanotube to remove Cr(VI) from wastewater with removal of the 92 % (Kim et al., 2024). Mpouras et al. (2021) investigated the use of multi wall carbon nanotubes for Cr(VI) removal from aqueous solutions with good results (Mpouras et al., 2021). Therefore, these results indicate that carbon nanotubes have a wide range of applications in the treatment Cr (VI) wastewater.

However, the application of carbon nanotubes in Cr(VI) wastewater treatment is limited owe to the high preparation cost (Hamzat et al., 2019). Therefore, a cheap raw material is needed to prepare the carbon nanotubes to reduce its production cost. Plastic waste is a kind of the pollutions, which has caused many environmental problems such as groundwater pollution and marine litter. Nowadays, plastic waste has

---

* Corresponding author.
  E-mail address: tbagmo@126.com (P. Liu).

become one of the major environment problem for the world (Chanthakett et al., 2021; Wang et al., 2024). Therefore, exploring the recycling of waste plastics has become an urgent problem that should be solved. At present, the treatment methods of the plastic waste mainly include waste incineration and landfill, mechanical recycling and chemical recycling (Ragaert et al., 2017). Compared with other methods, the chemical recycling method can recycle the energy and composition of waste plastics, realizing the comprehensive utilization of the waste plastics (Qureshi et al., 2020). Waste plastics contain the hydrocarbon elements, which can be used as the raw materials to prepare the carbon nanotubes. Cai et al. (2021) used the waste propylene as the raw material to prepare the carbon nanotubes and other high-value chemical products by catalytic cracking (Cai et al., 2021). Meanwhile, Li et al.(2023) successfully prepared carbon nanotubes using polyethylene as feedstock in the existence of the nickel-based catalyst (Li et al., 2023). In addition; Shen et al. (2022) successfully prepared the carbon nanotubes by microwave assisted pyrolysis of the waste plastics (Shen et al., 2022). Therefore, the production cost of carbon nanotubes can be reduced by the preparation method of pyrolytic waste plastics.

The physicochemical properties of the original carbon nanotubes hinder its application in Cr(VI) removal due to poor removal capacity (Hamzat et al., 2019; Hu et al., 2009). Dehghani et al. (2015) used the multi-walled carbon nanotubes and single-walled carbon nanotubes for Cr(VI) removal with the 1.26 and 2.35 mg g^{-1}, respectively (Dehghani et al., 2015). Combined carbon nanotubes with metallic oxide can improve Cr(VI) adsorption capacity of carbon nanotubes. Gupta et al. (2011) prepared the magnetic multi-walled carbon nanotubes for Cr(VI) removal from wastewater with good results, indicating that the presence of the iron oxide can enhance Cr(VI) removal (Gupta et al., 2011). Besides; it can realize magnetic recovery after use owe to the existence of iron oxide (Gupta et al., 2011). Recently, it has been reported that doping with nitrogen atoms is an effective method to enhance Cr(VI) removal (Lin et al., 2016). The reason is that nitrogen atoms can effectively modulate the charge density and basic sites on the surface of adsorbents. For example, the N-doped carbon-based composites have excellent removal of the Cr(VI). The reason is that the N-doping enhances electrostatic adsorption on the surface of carbon composites (Li et al., 2013). Meanwhile, N doping can improve the hydrophilicity of the adsorbent and enhance Cr(VI) removal (Cao et al., 2016; Huang et al., 2019). Therefore, the nitrogen doping can significantly enhance the adsorption and reduction capacity of adsorbents. The N-doped carbon nanotubes is often prepared using melamine, which can interact with a range of materials due to its unique structure (Zhong et al., 2015). However, melamine can cause adverse effects on living organisms (Chen et al., 2021). While, the urea can be used as the doping material to avoid its disadvantages due to non-toxic compared to the melamine.

In this work, the magnetic N/Fe doped carbon nanotubes (N/Fe-CNTs) is successfully prepared by pyrolysis of waste plastics in the existence of the urea using Fe(NO$_3$)$_3$ as catalyst for Cr(VI) removal from wastewater. The physicochemical properties of the N/Fe-CNTs are characterized and analyzed. The Cr(VI) removal capacity of the N/Fe-CNTs is also investigated. The Cr(VI) adsorption performance of the N/Fe-CNTs is analyzed. Besides, the possible involved Cr(VI) removal mechanism is discussed.

2. Experimental section

2.1. Material

Low density polyethylene (LDPE) and Fe(NO$_3$)$_3$·9H$_2$O (analytical grade) are purchased from the Sinopharm Chemical Reagent Co China. Urea (analytical grade) and K$_2$Cr$_2$O$_7$ (analytical grade, ≥99.8 % purity) are purchased from the Yantai Shuangshuang Chemical Co., Ltd, China. The 1,10-phenanthroline (C$_{12}$H$_8$N$_2$·H$_2$O) (analytical grade, >99 %) and Tert-butyl alcohol (>99 % purity) are obtained from the Macklin Chemical Co., Ltd, China.

2.2. Synthesis of N/Fe-CNTs

15 g Fe(NO$_3$)$_3$·9H$_2$O is dissolved into the ethanol solution, and then LDPE is impregnated with it. The mixture is dried at 80℃ for 24 h in the electric oven. Finally, the dried mixture is grinded with urea, which is heated at 800℃ for 2 h in the resistance furnace under nitrogen atmosphere. The residue in the resistance furnace is named as the N/Fe-CNTs. The preparation process of the N/Fe-CNTs is presented in Fig. 1. The characterization method of the N/Fe-CNTs is in the supporting material.

2.3. Cr(VI) adsorption process

The adsorption kinetics process are carried out using the magnetically mixing 0.2 g N/Fe-CNTs with 100 mL Cr(VI) (50 mg/L) in the 250 mL erlenmeyer flask. After stirring at 180 rpm for a certain time interval, the filtration is carried out through a 0.22 μm PTFE filter. Cr(VI) concentration is obtained using the UV–VIS spectroscopy at 540 nm. Adsorption amounts (q$_e$ and q$_t$) of Cr(VI) in the adsorption experiment are calculated from the following equation:

$$q_t = \frac{V(C_0 - C_t)}{M} \tag{1}$$

$$q_e = \frac{V(C_0 - C_e)}{M} \tag{2}$$

The C$_0$ and C$_t$ are the initial Cr(VI) concentration and Cr(VI) concentration over time, respectively. C$_e$ is the equilibrium concentration of Cr(VI). M and V are the quality of the N/Fe-CNTs and volume of the solution, respectively.

The experiment method of the adsorption isotherm is similar with the adsorption kinetic experiment, and the adsorption time is 24 h to achieve the adsorption equilibrium. The adsorption kinetic models and adsorption isotherm models are presented in Table S1 and Table S2, respectively.

3. Results and discussions

3.1. Microstructure analysis

Fig. 2 shows the microstructure analysis of the N/Fe-CNTs. As Fig. 2a-b shown, the carbon nanotubes are successfully prepared by pyrolysis of the LDPE. In addition, the results of the element mapping image show that the N and Fe element are successfully doped on the carbon nanotubes (Fig. 2c-d). The above result indicates the successful preparation of the N/Fe-CNTs.

3.2. XRD and FT-IR analysis

Fig. 3a shows the XRD analysis of the N/Fe-CNTs. The characteristic peaks of Fe$_3$C (2θ = 37.8°, 42.9°, 45.0°, 45.8°, 49.1°, 51.8°and 54.4°) are appeared in N/Fe-CNTs with good crystallinity (Zhao et al., 2019). Besides, both peaks of the Fe$_2$O$_3$ and Fe$_3$O$_4$ also exist on N/Fe-CNTs, indicating that the reduction of Fe oxides is incomplete in the preparation process of the N/Fe-CNTs (Zhao et al., 2020; Liu et al., 2023). Besides, the N/Fe-CNTs has the strong Fe^0 diffraction peak at 2θ = 44.7°. The appearance of graphite peak (2θ = 26.5°) may be due to the formation of CNTs with high graphiticity (Zhong et al., 2015). The adhesion between metal clusters and carbon atoms ensures the nucleation of nanotubes (Page et al., 2010). During LDPE pyrolysis process, the iron oxide is reduced into Fe^0 and reacts with carbon nitride to form Fe$_3$C (Huang et al., 2019). Besides, the small amount of Fe^0 and Fe^{2+} on N/Fe-CNTs is beneficial for stabilizing their own structure during adsorption process (Huang et al., 2019). The N/Fe-CNTs has the magnetism, which can be quickly recycled from wastewater.

The chemical composition of the N/Fe-CNTs is characterized by the FT-IR spectra. The peak near 3434 cm^{-1} is N–H or O–H group (Hao et al.,
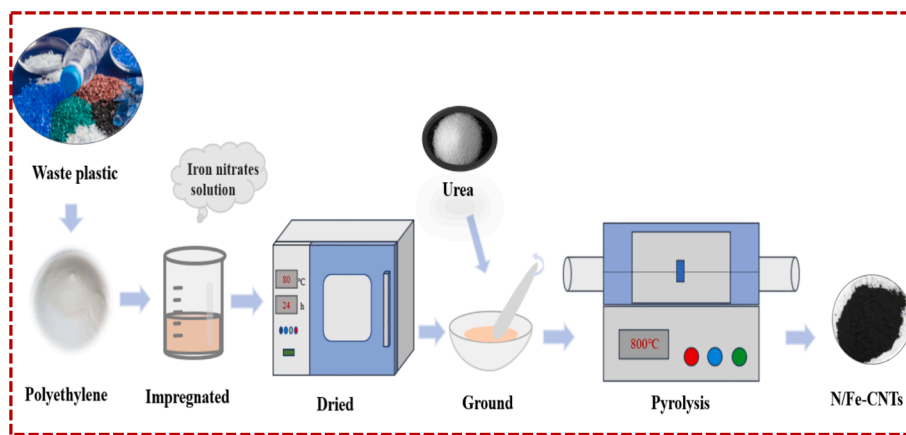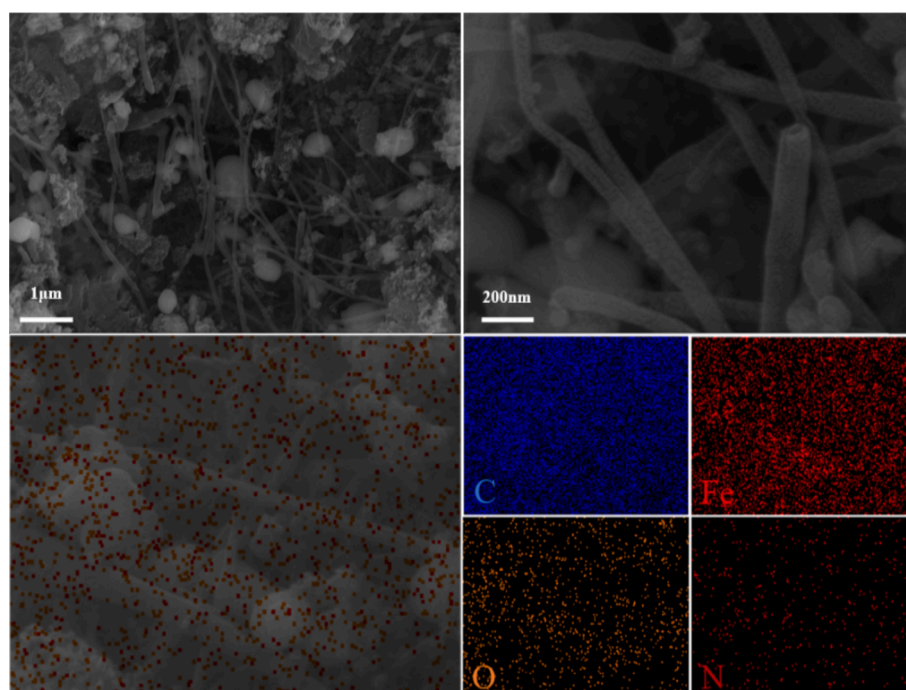
Fig. 1. The preparation process of the N/Fe-CNTs.

Fig. 2. SEM micrographs (a-b) and EDS (c-d) of the N/Fe-CNTs.

2010). The peak at 1622 cm^{-1} is N–H in-plane deformation vibrations or C=C stretching vibration (Li et al., 2013). The strong peak near 1164 cm^{-1} is related to the –C–O stretching vibration and –OH stretching vibration of phenolic hydroxyl groups and carboxyl groups (Yang et al., 2011). The characteristic peak near 590 cm^{-1} is the Fe–O bonds (Liu et al., 2023).

3.3. Pore structure and magnetism analysis of the N/Fe-CNTs

Fig. 4a shows the N$_2$-adsorption/desorption isotherm of the N/Fe-CNTs. The BET specific surface area (SSA), pore volume and average pore size are shown in Table 1. As Fig. 4a shown, the N$_2$ adsorption amount of the N/Fe-CNTs significantly increases at P/P$_0$ < 0.1, and then the curve tends to slowly increase. The "Hysteresis loop" appears on N/Fe-CNTs, indicating the mesoporous structure of N/Fe-CNTs. As Table 1 shown, SSA and total pore volume are 158.71 m^2 g^{-1} and 0.40 cm^3 g^{-1}, respectively with the average pore size of the 0.67 nm.

The hysteresis loop analysis of the N/Fe-CNTs is shown in Fig. 4b. As Fig. 4b shown, the saturation magnetization of the N/Fe-CNTs is 36.47 emu g^{-1}, indicating that N/Fe-CNTs has certain of the soft magnetic property. N/Fe-CNTs can be quickly separated and recovered from aqueous solution under the action of applied magnetic field (Alqadami et al., 2017).

3.4. Influence of pH

Fig. 5 shows the Cr(VI) removal behavior on N/Fe-CNTs at pH of 3–7. As Fig. 5 shown, the N/Fe-CNTs has large Cr(VI) adsorption amount at pH of 3–4. Cr(VI) has various of forms at different pH. At pH 2–5, Cr(VI) exists the formation of the HCrO$_4^-$, Cr$_2$O$_7^{2-}$, which possess the strong oxidizing properties (Su et al., 2020). Because of the difference in adsorption free energy and the increase in redox potential of the Cr(VI)/Cr(III) pair due to low pH, the low pH is generally more suitable for Cr(VI) reduction and removal (Wang et al., 2021; Hsu et al., 2009). Under strong acidic conditions, the H$^+$ participates in the redox reaction of surface functional groups with Cr(VI), which is mainly reduced into Cr(III) and produces OH$^-$ (Zhu et al., 2022). The OH$^-$ content in the solution increases, which constantly competes with chromium-containing
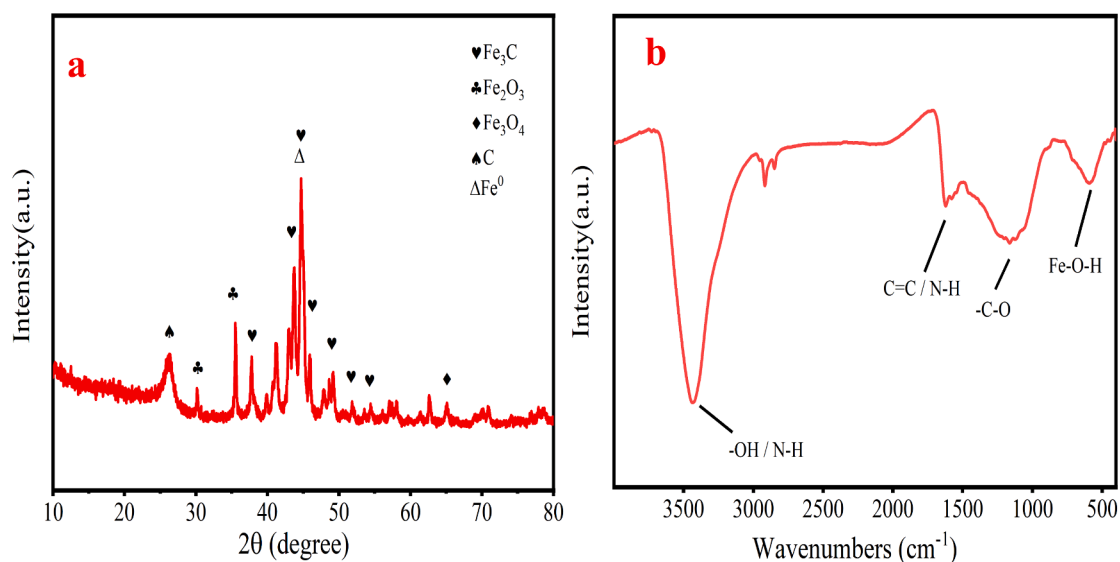
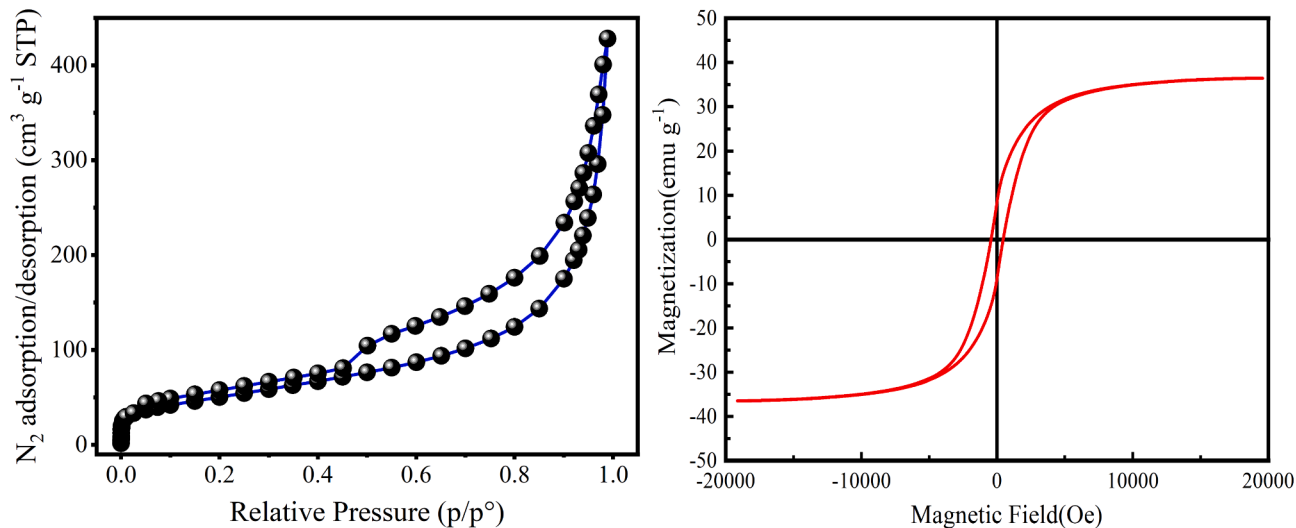**Fig. 3.** XRD pattern (a) and FT-IR spectra (b) of the N/Fe-CNTs.

Fig. 4. N$_2$-adsorption–desorption isotherm of N/Fe-CNTs (a) and the hysteresis loop of the N/Fe-CNTs (b).

Table 1
Pore structure of the N/Fe-CNTs.

Item	SSA (m^2/g)	Pore volume (cm^3 g^{-1})	Average pore size (nm)
N/Fe-CNTs	158.71	0.40	0.67

groups for the adsorption active sites, resulted in the Cr(VI) adsorption amount decrease (Shi et al., 2022). The zeta potential analysis indicates that the N/Fe-CNTs is positively charged at pH<5.5 and negatively charged at pH>5.5 (Fig. S1). The positively charged surface of the N/Fe-CNTs contributes to HCrO$_4^-$ adsorption due to electrostatic attraction. While the Cr(VI) adsorption amount is hindered due to electrostatic repulsion at pH>5.5. Therefore, the Cr(VI) adsorption amount is generally decrease with increasing in pH value. The N/Fe-CNTs has large Cr(VI) adsorption amount at pH = 3. Therefore, the desire pH for N/Fe-CNTs adsorption Cr(VI) is 3.

3.5. Adsorption isotherms study

The Cr(VI) adsorption behavior on N/Fe-CNTs is analyzed using the adsorption isotherms models (Qin et al., 2023). Fig. 6 shows the Cr(VI) adsorption data fitting adsorption isotherm models, and corresponded fitting results are shown in Table.2. The R^2 value of Cr(VI) adsorption data fitting the Hill model is 0.9957 (Table 2), which has large R^2 compared to the Langmuir, Freundlich and Temkin models. The n value calculated from Hill model for Cr(VI) is 1.2598, which indicates that 1.2598 Cr(VI) can be captured by one adsorption site of the N/Fe-CNTs. Cr(VI) adsorption amount is 27.47 mg g^{-1}, which is calculated from the Hill model

The parameter (K$_L$) of the Langmuir model can be used to calculate the dimensionless factor R$_L$. The calculated result of the R$_L$ value can be used to analyze the feasible of Cr(VI) adsorption (Cheng et al., 2021). The R$_L$ value is calculated based on the equation (3).

$$R_L = \frac{1}{1 + K_L C_0} \tag{3}$$

If the calculated result of the R$_L$ belongs to the 0–1, the Cr(VI) adsorption on N/Fe-CNTs is feasible. The R$_L$ values of Cr(VI) adsorption on N/Fe-CNTs is 0.2484–0.6231 based on calculation. This result demonstrates the feasible of the Cr(VI) adsorption on N/Fe-CNTs.
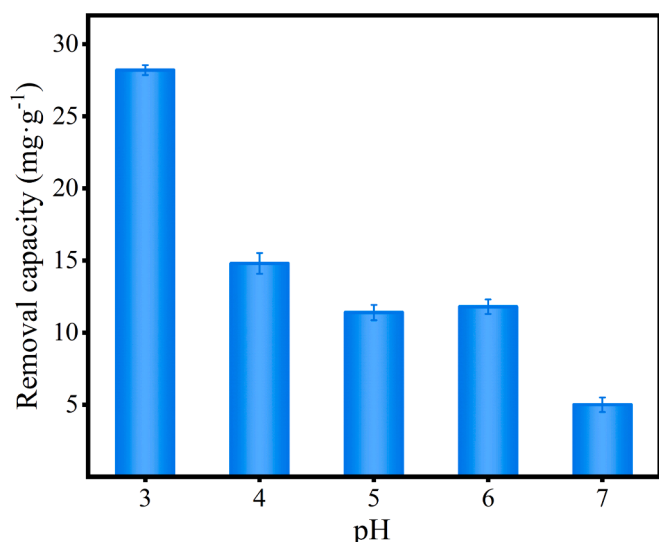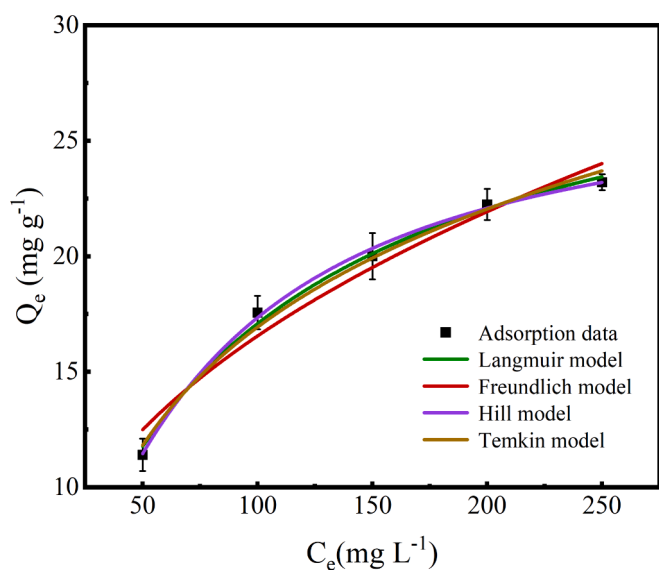
Fig. 5. The influence of pH on Cr(VI) removal.

Fig. 6. Cr(VI) adsorption data fitting the adsorption isotherm models.

Table 2
The calculated results of adsorption isotherm models.

Models	Parameter	Value Cr(VI)
Langmuir	q_m (mg/g)	31.17
	K_L (L/mg)	0.0121
	R^2	0.9931
Freundlich	1/n	0.4065
	K_F ((mg/g).(L/mg)$^{1/n}$)	2.545
	R^2	0.9520
Hill	Q_m	27.47
	n	1.259
	K	65.27
	R^2	0.9957
Temkin	K_T (L/g)	0.0091
	B_T(J/mol)	7.38
	R^2	0.9872

The Cr(VI) adsorption amount of other similar adsorbents is summarized in Table S3, which is used to compared with N/Fe-CNTs. As Table S3 shown, N/Fe-CNTs has large Cr(VI) adsorption amount compared to other similar adsorbents. Therefore, N/Fe-CNTs can be used as the promising adsorbent for Cr(VI) treatment from wastewater.

3.6. Adsorption kinetics study

Pseudo-first order, Pseudo-second order and Intraparticle diffusion models are used to investigate Cr(VI) adsorption behavior on N/Fe-CNTs. Table 3 lists the calculated results of the Cr(VI) adsorption behavior on N/Fe-CNTs. As shown in Table 3, compared with the Pseudo-first order and Intraparticle diffusion models, the Cr(VI) adsorption data fitting the Pseudo-second order has the large correlation coefficient (R^2) value of 0.9993. Therefore, the Cr(VI) adsorption kinetic process can be accurately explained by the Pseudo-second order model. This result also demonstrates that the chemical adsorption involves into Cr(VI) adsorption process (Cheng et al., 2022). The Cr(VI) adsorption data fitting Pseudo-second-order model is shown in Fig. 7. Besides, the Intraparticle diffusion model is used to further analyze the rate-limiting step of the Cr(VI) adsorption on N/Fe-CNTs. The C value of Cr(VI) adsorption on N/Fe-CNTs is 8.77, which is calculated from Intraparticle diffusion mode. This result demonstrates that the Intraparticle diffusion isn't alone rate-limiting step for Cr(VI) adsorption on N/Fe-CNTs.

3.7. Cr(VI) removal mechanism

Fig. 8a indicates that the Cr element is found on N/Fe-CNTs based on SEM-EDS analysis. This result demonstrates that the Cr element is successfully adsorbed on N/Fe-CNTs. The XPS survey spectrum of the N/Fe-CNTs also appears the Cr element, indicating that Cr(VI) is successfully adsorbed by N/Fe-CNTs (Fig. 8b). The comparison of XPS survey spectra before and after Cr(VI) adsorption implies that the Fe participates in Cr (VI) removal process due to the decrease of Fe content (Fig. 8b). Fig. 8c-d show the C 1 s peaks of N/Fe-CNTs before and after Cr(VI) adsorption. The peaks at 283.07, 284.8 and 288.21 eV are C–C/C=C, C–O and C=O group, respectively (Tang et al., 2021). For the N/Fe-CNTs, upon reaction with Cr(VI), the percentage of C=O decreases from 7.5 % to 7.26 %, indicating that the –CHO group is an electron donor that is oxidized to –COOH by Cr(VI) (Eq.4) (Zhang et al., 2020). Generally, the C-O group is the adsorption and reduction site of the N/Fe-CNTs, and the adsorption and reduction simultaneously occur (Liu et al., 2023) (Eq.5). However, the proportion of the C-O group decreases. The XPS spectrum of N1s is deconvoluted into three peaks of the pyridinic N, graphitic N, and N-O at 397.84 eV, 400.28 eV, and 403.88 eV, respectively (Fig. 8e-f) (Cai et al., 2021). Compared with the signal peaks of nitrogen in the N/Fe-CNTs, the content of nitrogen-oxides and pyridinic-N decreases. While, the content of graphitic-N increases. This result indicates that the redox reaction between Cr(VI) and nitrogen groups on N/Fe-CNTs occurs (Lin et al., 2016). Based on XPS analysis, it confirms that the presence of nitrogen functional groups in N/Fe-CNTs involves into the Cr(VI) removal. Covalently linked nitrogen functional groups are Lewis base

Table 3
The calculated results of adsorption kinetics models.

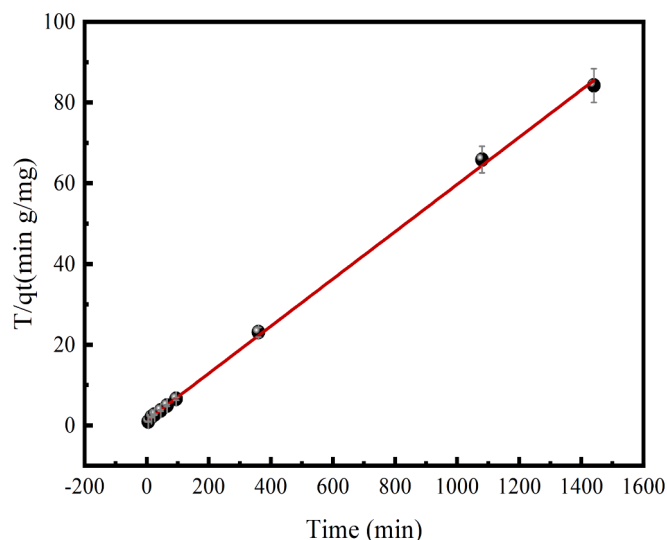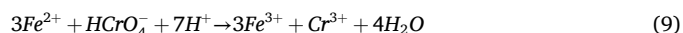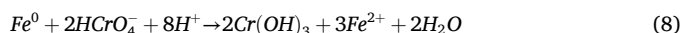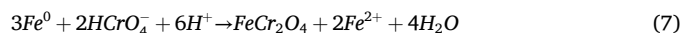| Model	Parameter	Value Cr(VI)
Pseudo-first order	$q_{e.cal}$ (mg/g)	15.76
	K_1 (1/min)	0.037
	R^2	0.8990
Pseudo-second order	$q_{e.cal}$ (mg/L)	17.08
	K_2 (g/mg min)	1.1991
	R^2	0.9993
Intraparticle diffusion	C (mg/g)	8.77
	K_3 (mg/g min$^{1/2}$)	0.2558
	R^2	0.6042

Fig. 7. Cr(VI) adsorption data fitting Pseudo-second order.

active sites for binding. Therefore, nitrogen functional groups in N/Fe-CNTs favors Cr(VI) removal (Li et al., 2013).

$$3R - CHO + 2HCrO_4^- + 8H^+ \rightarrow 3R - COOH + 2Cr^{3+} + 5H_2O \tag{4}$$

$$R - CH_2OH + HCrO_4^- + 4H^+ \rightarrow R - COOH + Cr^{3+} + 3H_2O \tag{5}$$

Both Fe^0 and Fe^{2+} are reducing substances in the N/Fe-CNTs (Li et al., 2019). As shown in the Eq.6–8, Fe^0 can reduce $HCrO_4^-$ into the Cr^{3+}, $FeCr_2O_4$ and $Cr(OH)_3$ due to fact that Fe^0 can reduce the charge transfer of $HCrO_4^-$ in acidic solution (Liu et al., 2023). While; the Fe^0 is oxidized into the Fe^{2+}. The Fe^{2+} can also reduce Cr (VI) and subsequently produce Cr^{3+} (Eq.9) due to fact that the standard reduction potential of Fe^{3+}/Fe^{2+} is less than that of Cr^{6+}/Cr^{3+} (Liu et al., 2023). As shown in Fig. 8g-h, the Fe^0 peak area decreases from 29.47 % to 23.57 % after reaction. While, the Fe^{3+} peak area increases from 23.64 % to 28.39 % after reaction. These results indicate that Fe^0 participates in Cr (VI) removal. However, the Fe^{2+} peak area increases from 46.92 % to 48.04 %, which may be due to the incomplete oxidation of excess Fe^{2+} converted from Fe^0. The hydrolysis of Fe^{2+} increases the H^+

concentration in aqueous solution (Eq.10). Meanwhile, it favors the accumulation of more Cr^{3+} on N/Fe-CNTs as the acidity of the solution increases. In addition, the reducing radicals such as H^* and $-O_2^-$ are generated during Fe^0 corrosion, and the H^* can indirectly reduce Cr(VI) into Cr^{3+} (Eqs.11–12) (Yang et al., 2021; Li et al., 2019).

$$3Fe^0 + 2HCrO_4^- + 14H^+ \rightarrow 2Cr^{3+} + 3Fe^{2+} + 8H_2O \tag{6}$$

$$3Fe^0 + 2HCrO_4^- + 6H^+ \rightarrow FeCr_2O_4 + 2Fe^{2+} + 4H_2O \tag{7}$$

$$Fe^0 + 2HCrO_4^- + 8H^+ \rightarrow 2Cr(OH)_3 + 3Fe^{2+} + 2H_2O \tag{8}$$

$$3Fe^{2+} + HCrO_4^- + 7H^+ \rightarrow 3Fe^{3+} + Cr^{3+} + 4H_2O \tag{9}$$

$$3Fe^{2+} + 4H_2O \rightarrow Fe_3O_4 + H_2 + 6H^+ \tag{10}$$

$$Fe^0 + 2H^+ \rightarrow Fe^{2+} + 2H^* \tag{11}$$

$$3H^* + Cr^{6+} \rightarrow Cr^{3+} + 3H^+ \tag{12}$$

The Cr 2p spectra analysis is elucidated (Fig. 8h). Two peaks of Cr $2p_{1/2}$ and Cr $2p_{3/2}$ appear at 589.03 eV and 579.45 eV, respectively. The peaks at 576.93 and 586.52 eV indicate the presence of Cr(III), suggesting that Cr(VI) is partially reduced into Cr(III) (Luo et al., 2021). Therefore, adsorption and reduction reaction are important ways for Cr (VI) removal from wastewater.

3.8. Quantitative analysis of Cr(VI) removal

In order to investigate the contribution of different removal mechanisms for Cr(VI) removal, bursting experiments are carried out using TBA (Tert-butyl alcohol) and 0.1 g/L 1,10-phenanthroline for H^* and Fe^{2+}, respectively. In order to quantify the contribution of Fe for Cr(VI) removal, 15 wt% HCl solution is used to dissolve the Fe from N/Fe-CNTs (Li et al., 2019; Zheng et al., 2022). Finally, the respective contribution to Cr(VI) removal can be obtained using the following equation. The Cr (VI) removal decreases by 4.3 % (23.6 % of total removal efficiency) with the existence of the 1, 10-phenanthroline. It indicates that the dissolved Fe^{2+} contributes to Cr(VI) removal by reduction. However, the Cr (VI) removal slightly reduces by 3.7 % after adding TBA. It indicates a contribution of 20.3 % to the total removal efficiency of H^*. According to Eq.13, the contribution of Fe^0 for Cr (VI) removal is calculated to be
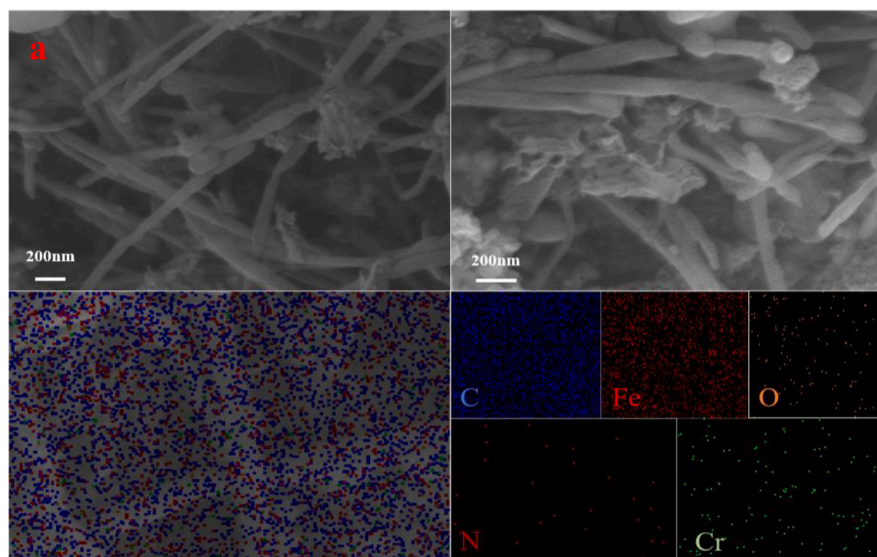

Fig. 8. SEM-EDS analysis after Cr(VI) adsorption (a), XPS survey spectra of the N/Fe-CNTs after adsorption Cr(VI)(b), C 1 s spectra analysis before and after Cr(VI) adsorption(c-d), N 1 s spectra analysis before and after Cr(VI) adsorption(e-f), Fe 2p spectra analysis before and after Cr(VI) adsorption (g-h) and Cr 2p spectra analysis is elucidated (i).
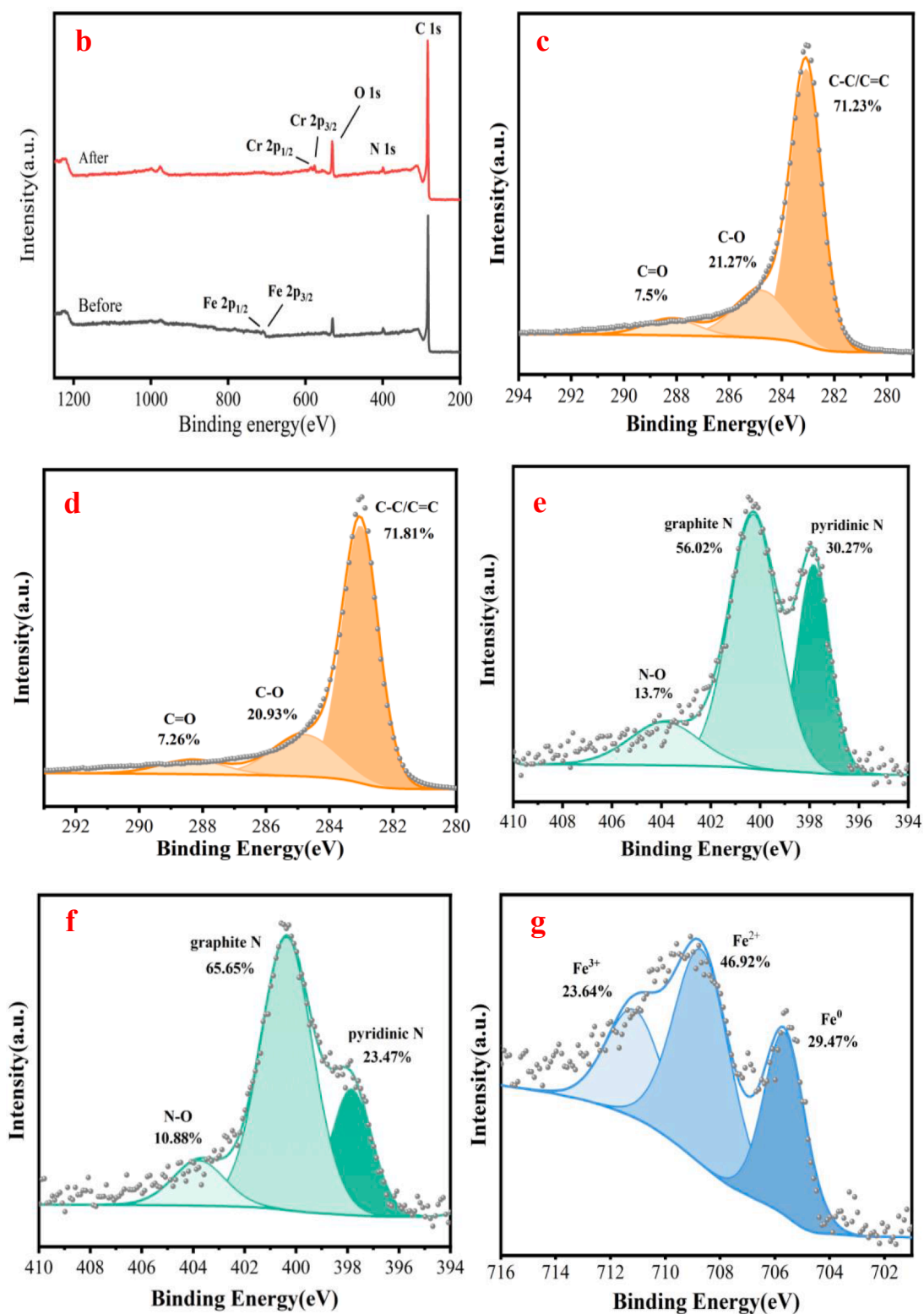
Fig. 8. (*continued*).

0.8 % (4.4 % of total removal efficiency). This may be because that N/Fe-CNTs has a certain protective effect on Fe^0, which limits its related reactions. According to the equation, the contribution of O-containing group to Cr (VI) removal is 1.54 % (8.5 % of total removal efficiency) (Eq.14). In Equations 13–14, R(Total) represents the total removal efficiency of 18.2 %. While, R(Fe^{2+}) represents removal due to Fe^{2+} and R(HCl) represents removal by HCl pretreatment. Fig. 9 shows that other

removal mechanism such as adsorption, pore filling, containing O and N groups account for 43.2 % of the total Cr (VI) removal. Therefore, the reduction of Fe^{2+}, H* and other removal mechanism are important parameters, which influences the Cr (VI) removal.

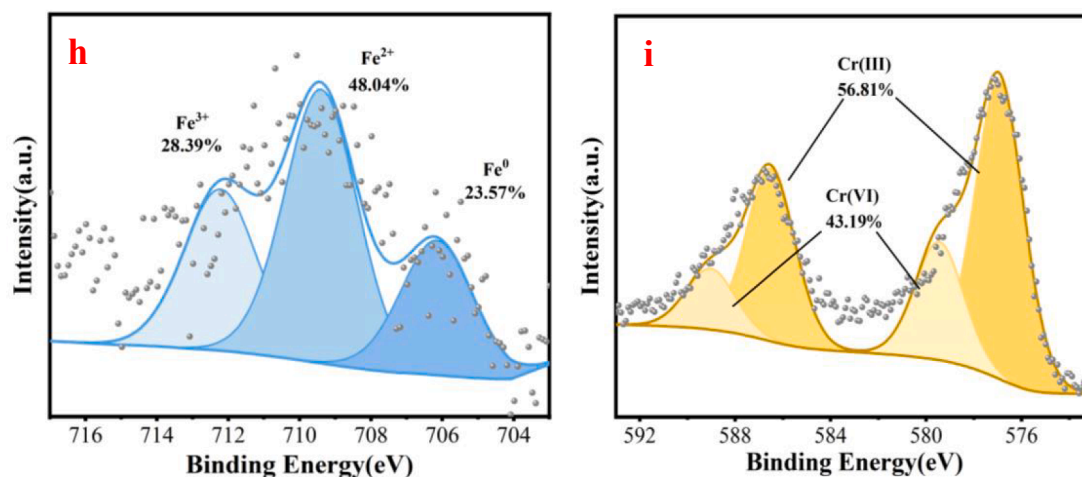$$R\left(Fe^0\right) = R(Total) - R(HCl) - R\left(Fe^{2+}\right) - R(H^*) \tag{13}$$

Fig. 8. (continued).

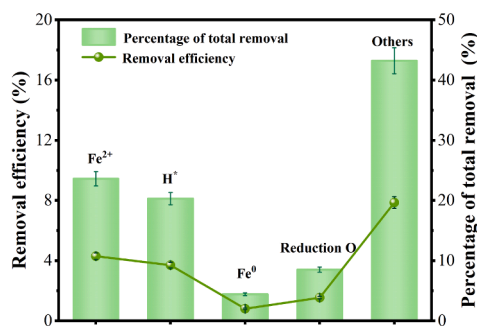**Fig. 9.** Quantitative analysis of Cr(VI) removal.

$$R(O) = R(Total) \times reduction efficiency - R(Fe^{2+}) - R(H^*) - R(Fe^0) \quad (14)$$

3.9. Explore Cr(VI) adsorption process

The binding energies of these groups (–COOH, –OH, and graphitic N) of the N/Fe-CNTs interaction with Cr(VI) are calculated using DFT. The calculated result is shown in Fig.S2. As Fig.S2 shown, it exists energy barrier in Cr(VI) adsorption process based on calculated result. Binding energies of Cr(VI) interactions with –COOH group is the most negative than that of the –OH and graphitic N groups. This result indicates that-COOH group plays a critical role in Cr(VI) adsorption.

4. Conclusions

N/Fe-CNTs is successfully prepared by one-pot pyrolysis method using urea as nitrogen dopant mixed with plastic waste in the existence of the iron-based catalyst. The specific surface area of the carbon nanotubes is 158.71 m^2/g and the saturation magnetization is 36.47 emu g^{-1}, contributing to Cr(VI) removal. The N/Fe-CNTs has large Cr (VI) adsorption amount at pH = 3, indicating that N/Fe-CNTs has effective Cr(VI) removal performance at low pH. The Cr (VI) adsorption capacity is 27.47 mg g^{-1}, based on Hill model calculation. The adsorption data can be accurately analyzed by the Pseudo-second order model, demonstrating chemisorption of Cr(VI). The –COOH, –OH groups and nitrogen-containing group in N/Fe-CNTs involve in Cr (VI) removal. While, the Fe^0, Fe^{2+}, H* and active substances containing O and N groups can reduce Cr (VI) into Cr (III). Quantitative calculation of Cr(VI) removal is investigated, indicating that the dissolved Fe^{2+} accounts for 23.6 % of the overall Cr(VI) removal.

CRediT authorship contribution statement

Song Cheng: Writing – original draft, Methodology, Investigation, Funding acquisition. **Xiangwang Zeng:** Writing – original draft, Resources, Methodology, Funding acquisition. **Peng Liu:** Supervision, Investigation.

Declaration of competing interest

The authors declare that they have no known competing financial interests or personal relationships that could have appeared to influence the work reported in this paper.

Acknowledgments

Appendix A. Supplementary data

Supplementary data to this article can be found online at https://doi.org/10.1016/j.arabjc.2024.105956.

References

Afzali, D., Fayazi, M., 2016. Deposition of MnO_2 nanoparticles on the magnetic halloysite nanotubes by hydrothermal method for lead(II) removal from aqueous solutions. J. Taiwan Inst. Chem. Eng. 63, 421–429.

Alqadami, A.A., Naushad, M., Abdalla, M.A., Ahamad, T., Abdullah Alothman, Z., Alshehri, S.M., Ghfar, A.A., 2017. Efficient removal of toxic metal ions from wastewater using a recyclable nanocomposite: A study of adsorption parameters and interaction mechanism. J. Clean. Prod. 156, 426–436.

Cai, N., Xia, S., Li, X., Xiao, H., Chen, X., Chen, Y., Bartocci, P., Chen, H., Williams, P.T., Yang, H., 2021. High-value products from ex-situ catalytic pyrolysis of polypropylene waste using iron-based catalysts: the influence of support materials. Waste Manag. 136, 47–56.

Cao, Y., Huang, J., Li, Y., Qiu, S., Liu, J., Khasanov, A., Khan, M.A., Young, D.P., Peng, F., Cao, D., Peng, X., Hong, K., Guo, Z., 2016. One-pot melamine derived nitrogen doped magnetic carbon nanoadsorbents with enhanced chromium removal. Carbon 109, 640–649.

Chanthakett, A., Arif, M.T., Khan, M.M.K., Oo, A.M.T., 2021. Performance assessment of gasification reactors for sustainable management of municipal solid waste. J. Environ. Manage. 291, 112661.

Chen, S., Yang, W., Zhang, X., Jin, J., Liang, C., Wang, J., Zhang, J., 2021. Melamine induces reproductive dysfunction via down-regulated the phosphorylation of p38 and downstream transcription factors Max and Sap1a in mice testes. Sci. Total Environ. 770, 144727.

Cheng, S., Xing, B., Shi, C., Nie, Y., Xia, H., 2021. Efficient and selective removal of Pb(II) from aqueous solution by modification crofton weed: Experiment and density functional theory calculation. J. Clean. Prod. 280.

Cheng, S., Zhao, S., Guo, H., Xing, B., Liu, Y., Zhang, C., Ma, M., 2022. High-efficiency removal of lead/cadmium from wastewater by MgO modified biochar derived from crofton weed. Bioresour. Technol. 343.

Dehghani, M.H., Taher, M.M., Bajpai, A.K., Heibati, B., Tyagi, I., Asif, M., Agarwal, S., Gupta, V.K., 2015. Removal of noxious Cr (VI) ions using single-walled carbon nanotubes and multi-walled carbon nanotubes. Chem. Eng. J. 279, 344–352.

Fayazi, M., 2020. Removal of mercury(II) from wastewater using a new and effective composite: sulfur-coated magnetic carbon nanotubes. Environ. Sci. Pollut. Res. 27, 12270–12279.

Fayazi, M., Ghanbarian, M., 2020. One-pot hydrothermal synthesis of polyethylenimine functionalized magnetic clay for efficient removal of noxious Cr(VI) from aqueous solutions. Silicon 12, 125–134.

Fida, H., Guo, S., Zhang, G., 2015. Preparation and characterization of bifunctional Ti–Fe kaolinite composite for Cr(VI) removal. J. Colloid Interface Sci. 442, 30–38.

Fu, F., Wang, Q., 2011. Removal of heavy metal ions from wastewaters: A review. J. Environ. Manage. 92, 407–418.

Guan, D., Zhao, J., Wang, Y., Fu, Z., Zhang, D., Zhang, H., Xie, J., Sun, Y., Zhu, J., Wang, D., 2024. A critical review on sustainable management and resource utilization of digestate. Process Saf. Environ. Prot. 183, 339–354.

Guo, H., Cheng, S., Xing, B., Meng, M., Feng, L., Nie, Y., Zhang, C., 2024. Preparation of three kinds of efficient sludge-derived adsorbents for metal ions and organic wastewater purification. Arab. J. Chem. 17, 105671.

Gupta, V.K., Agarwal, S., Saleh, T.A., 2011. Chromium removal by combining the magnetic properties of iron oxide with adsorption properties of carbon nanotubes. Water Res. 45, 2207–2212.

Hamzat, W.A., Abdulkareem, A.S., Bankole, M.T., Tijani, J.O., Kovo, A.S., Abubakre, O. K., 2019. Adsorption studies on the treatment of battery wastewater by purified carbon nanotubes (P-CNTs) and polyethylene glycol carbon nanotubes (PEG-CNTs). J. Environ. Sci. Health A 54, 827–839.

Hao, G.P., Li, W.C., Qian, D., Lu, A.H., 2010. Rapid synthesis of nitrogen-doped porous carbon monolith for CO2 capture. Adv. Mater. 22, 853–857.

Hsu, N.H., Wang, S.L., Lin, Y.C., Sheng, G.D., Lee, J.F., 2009. Reduction of Cr(VI) by crop-residue-derived black carbon. Environ. Sci. Tech. 43, 8801–8806.

Hu, J., Chen, C., Zhu, X., Wang, X., 2009. Removal of chromium from aqueous solution by using oxidized multiwalled carbon nanotubes. J. Hazard. Mater. 162, 1542–1550.

Huang, J., Cao, Y., Wen, H., Zhang, J., Wang, H., Yu, H., Peng, F., 2019. Unraveling the intrinsic enhancement of fluorine doping in the dual-doped magnetic carbon adsorbent for the environmental remediation. J. Colloid Interface Sci. 538, 327–339.

Huang, J., Cao, Y., Qin, B., Zhong, G., Zhang, J., Yu, H., Wang, H., Peng, F., 2019. Highly efficient and acid-corrosion resistant nitrogen doped magnetic carbon nanotubes for the hexavalent chromium removal with subsequent reutilization. Chem. Eng. J. 361, 547–558.

Kim, S.B., Lee, S.Y., Park, S.J., 2024. TiO2/Multi-walled carbon nanotube electrospun nanofibers mats for enhanced Cr(VI) photoreduction. J. Clean. Prod. 448, 141611.

Li, J., Lan, H., Liu, H., Zhang, G., An, X., Liu, R., Qu, J., 2019. Intercalation of nanosized Fe3C in iron/carbon to construct multifunctional interface with reduction, catalysis, corrosion resistance, and immobilization capabilities. ACS Appl. Mater. Interfaces 11, 15709–15717.

Li, Q.L., Shan, R., Wang, S.X., Yuan, H.R., Chen, Y., 2023. Carbon nanotubes production from catalytic pyrolysis of polyethylene over nickel-based catalysts: The influence of support materials. Fuel 343, 127966.

Li, Y., Zhu, S., Liu, Q., Chen, Z., Gu, J., Zhu, C., Lu, T., Zhang, D., Ma, J., 2013. N-doped porous carbon with magnetic particles formed in situ for enhanced Cr(VI) removal. Water Res. 47, 4188–4197.

Lin, F., Wang, Y., Lin, Z., 2016. One-pot synthesis of nitrogen-enriched carbon spheres for hexavalent chromium removal from aqueous solution. RSC Adv. 6, 33055–33062.

Liu, K., Zhao, D., Hu, Z., Xiao, Y., He, C., Jiang, F., Zhao, N., Zhao, C., Zhang, W., Qiu, R., 2023. The adsorption and reduction of anionic Cr(VI) in groundwater by novel iron carbide loaded on N-doped carbon nanotubes: Effects of Fe-confinement. Chem. Eng. J. 452, 139357.

Luo, Q., Huang, X., Luo, Y., Yuan, H., Ren, T., Li, X., Xu, D., Guo, X., Wu, Y., 2021. Fluorescent chitosan-based hydrogel incorporating titanate and cellulose nanofibers modified with carbon dots for adsorption and detection of Cr(VI). Chem. Eng. J. 407, 127050.

Ma, C., Liu, D., Deng, S., Vakili, M., 2024. Efficient chromium (VI) removal with zirconium oxide-carbon nanotubes via filtration-steam hydrolysis. Chem. Eng. Res. Des. 204, 664–672.

Mpouras, T., Polydera, A., Dermatas, D., Verdone, N., Vilardi, G., 2021. Multi wall carbon nanotubes application for treatment of Cr(VI)-contaminated groundwater; modeling of batch & column experiments. Chemosphere 269, 128749.

Myers, C.R., 2012. The effects of chromium(VI) on the thioredoxin system: Implications for redox regulation. Free Radic. Biol. Med. 52, 2091–2107.

Page, A.J., Yamane, H., Ohta, Y., Irle, S., Morokuma, K., 2010. QM/MD simulation of SWNT nucleation on transition-metal carbide nanoparticles. J. Am. Chem. Soc. 132, 15699–15707.

Qin, X., Cheng, S., Xing, B., Qu, X., Shi, C., Meng, W., Zhang, C., Xia, H., 2023. Preparation of pyrolysis products by catalytic pyrolysis of poplar: Application of biochar in antibiotic wastewater treatment. Chemosphere 338, 139519.

Qureshi, M.S., Oasmaa, A., Pihkola, H., Deviatkin, I., Tenhunen, A., Mannila, J., Minkkinen, H., Pohjakallio, M., Laine-Ylijoki, J., 2020. Pyrolysis of plastic waste: Opportunities and challenges. J. Anal. Appl. Pyrol. 152, 104804.

Ragaert, K., Delva, L., Van Geem, K., 2017. Mechanical and chemical recycling of solid plastic waste. Waste Manag. 69, 24–58.

Shen, X., Zhao, Z., Li, H., Gao, X., Fan, X., 2022. Microwave-assisted pyrolysis of plastics with iron-based catalysts for hydrogen and carbon nanotubes production. Mater. Today Chem. 26, 101166.

Shi, R., Liu, T., Lu, J., Liang, X., Ivanets, A., Yao, J., Su, X., 2022. Fe/C materials prepared by one-step calcination of acidified municipal sludge and their excellent adsorption of Cr(VI). Chemosphere 304, 135303.

Su, Q., Su, Z., Xie, W., Tian, C., Su, X., Lin, Z., 2020. Preparation of 2D nitrogen-doped magnetic Fe3C/C by in-situ self-assembled double-template method for enhanced removal of Cr(VI). Environ. Pollut. 263, 114374.

Tang, J., Zhao, B., Lyu, H., Li, D., 2021. Development of a novel pyrite/biochar composite (BM-FeS2@BC) by ball milling for aqueous Cr(VI) removal and its mechanisms. J. Hazard. Mater. 413, 125415.

Wang, Y., Lin, N., Gong, Y., Wang, R., Zhang, X., 2021. Cu–Fe embedded cross-linked 3D hydrogel for enhanced reductive removal of Cr(VI): Characterization, performance, and mechanisms. Chemosphere 280, 130663.

Wang, Y., Zhao, J., Fu, Z., Guan, D., Zhang, D., Zhang, H., Zhang, Q., Xie, J., Sun, Y., Wang, D., 2024. Innovative overview of the occurrence, aging characteristics, and ecological toxicity of microplastics in environmental media. Environ. Pollut. 346, 123623.

Xu, H., Zhang, H., Qin, C., Li, X., Xu, D., Zhao, Y., 2024. Groundwater Cr(VI) contamination and remediation: A review from 1999 to 2022. Chemosphere 360, 142395.

Yang, S.T., Wang, H., Wang, Y., Wang, Y., Nie, H., Liu, Y., 2011. Removal of carbon nanotubes from aqueous environment with filter paper. Chemosphere 82, 621–626.

Yang, Q., Wang, H., Li, F., Dang, Z., Zhang, L., 2021. Rapid and efficient removal of Cr (vi) by a core–shell magnetic mesoporous polydopamine nanocomposite: roles of the mesoporous structure and redox-active functional groups. J. Mater. Chem. A 9, 13306–13319.

Zhang, Y., Liu, N., Yang, Y., Li, J., Wang, S., Lv, J., Tang, R., 2020. Novel carbothermal synthesis of Fe, N co-doped oak wood biochar (Fe/N-OB) for fast and effective Cr(VI) removal. Colloids Surf A Physicochem Eng Asp 600, 124926.

Zhao, N., Chang, F., Hao, B., Yu, L., Morel, J.L., Zhang, J., 2019. Removal of organic dye by biomass-based iron carbide composite with an improved stability and efficiency. J. Hazard. Mater. 369, 621–631.

Zhao, L., Li, C., Li, H., Shu, Z., Luo, Y., Yang, H., Chen, Q., Xu, W., Zhang, W., Tan, X., 2024. Efficient Cr(VI) removal by pyrite/porous biochar: Critical role of potassium salt and sulphur. Environ. Pollut. 346, 123641.

Zhao, N., Liu, K., He, C., Gao, J., Zhang, W., Zhao, T., Tsang, D.C.W., Qiu, R., 2020. Singlet oxygen mediated the selective removal of oxytetracycline in C/Fe3C/Fe0 system as compared to chloramphenicol. Environ. Int. 143, 105899.

Zhao, N., Zhao, C., Tsang, D.C.W., Liu, K., Zhu, L., Zhang, W., Zhang, J., Tang, Y., Qiu, R., 2021. Microscopic mechanism about the selective adsorption of Cr(VI) from salt solution on O-rich and N-rich biochars. J. Hazard. Mater. 404, 124162.

Zheng, N., Zhou, Q., Wang, R., Lian, Y., He, X., Hu, R., Hu, Z., 2022. Rust triggers rapid reduction of Cr^{6+} by red phosphorus: The importance of electronic transfer medium of Fe^{3+}. Chemosphere 303, 134971.

Zhong, G., Wang, H., Yu, H., Peng, F., 2015. Nitrogen doped carbon nanotubes with encapsulated ferric carbide as excellent electrocatalyst for oxygen reduction reaction in acid and alkaline media. J. Power Sources 286, 495–503.

Zhu, Q., Gao, H., Sun, Y., Xiang, Y., Liang, X., Ivanets, A., Li, X., Su, X., Lin, Z., 2022. Highly efficient adsorption of chromium on N, S-codoped porous carbon materials derived from paper sludge. Sci. Total Environ. 834, 155312.

Zou, H., Zhao, J., He, F., Zhong, Z., Huang, J., Zheng, Y., Zhang, Y., Yang, Y., Yu, F., Bashir, M.A., Gao, B., 2021. Ball milling biochar iron oxide composites for the removal of chromium (Cr(VI)) from water: Performance and mechanisms. J. Hazard. Mater. 413, 125252.